JOURNAL OF PROPULSION AND POWER
Vol 8, No. 2, March–April 1992

Response of Propellant Combustion to a Turbulent Acoustic Boundary Layer

Robert A. Beddini* and Ted A. Roberts†
University of Illinois at Urbana-Champaign, Urbana, Illinois 61801

An analysis of the transitional and turbulent reactive acoustic boundary layer on a homogeneous, solid-propellant surface is conducted to investigate potential mechanisms of combustion instability. The theoretical approach utilizes a low Reynolds number turbulence closure model and a finite-difference solution procedure for an equation system of parabolic form. A new technique is developed for the condensed-phase thermal layer, in which the propellant space is mapped onto the gas space and efficiently solved using the same adaptive numerical grid. Results are obtained at an acoustic pressure node in the absence of a mean axial flow. The results indicate that acoustically induced transition can occur at relatively low acoustic pressure amplitudes, propellant response to harmonic axial velocity fluctuations is both rectified and displays a mean augmentation ("D-C shift"), and that nominal propellant combustion parameters lead to increasing susceptibility to acoustic transition at elevated mean pressures.

Nomenclature

A_s = pre-exponential constant in surface reaction
a_0 = unperturbed sonic speed
B_g = pre-exponential constant in gas-phase reaction
c_p = specific heat at constant pressure
c_π = specific heat of condensed phase
f = frequency, Hz
H = total enthalpy, $h + u^i u_i/2$
h = specific sensible enthalpy
h_α^0 = heat of formation of species α
k = thermal conductivity
k_s = equivalent sand roughness height
L_s^0 = heat of (dissociative) evaporation or sublimation
M = Mach number defined using a_0
n = normal burning rate pressure exponent
p = static pressure
q = turbulence intensity, $\overline{(u'^i u_i')}^{1/2}$
R = inner radius of a cylindrical duct
Re_{ac} = axial acoustic Reynolds number, $\overline{u_c''}/(f/\bar{\nu}_c)^{1/2}$
Re_s = injection Reynolds number, $\bar{\rho}_s \bar{v}_s \delta/\bar{\mu}_s$
Re_t = turbulence Reynolds number, $\rho\, q\, \Lambda/\mu$
R_u = universal gas constant
r = radial distance from centerline
$\dot{r}$ = condensed phase surface regression rate
T = static temperature
T_A = activation temperature
t = time
u_j = velocity vector (u, v, w)
W_{av} = average molecular weight
x_j = coordinate vector
Y_α = species mass fraction
y = distance from surface, $\delta - r$ (planar flow) or $R - r$ (axisymmetric flow)
α = index for chemical species
α_π = thermal diffusivity of the condensed phase, $k_\pi/(\rho_\pi c_\pi)$
β_g = temperature exponent of gas-phase reaction pre-exponential coefficient
Δh_g = heat of reaction per unit mass
δ_a = noninjected laminar acoustic boundary-layer thickness, $(\nu/f)^{1/2}$
δ_{aa} = actual injected acoustic boundary-layer thickness
δ_f = normalized flame height, $k_s/\dot{m}c_p$
ζ_π = linear stretching factor used in condensed-phase mapping
η = condensed-phase coordinate
Λ = turbulence macrolength scale
μ = viscosity
ν = kinematic viscosity
ρ = density
σ = k/c_p
σ_v = $[\overline{v_s' v_s'}/\bar{v}_s^2]^{1/2}$
τ = normalized time, $f \times t$, cycles
Φ = concentration (pressure) exponent in reaction rate
ϕ = characteristic length scale
ω = specific reaction source term
ϑ = index for planar or axisymmetric geometry

Subscripts

a = acoustic
c = duct centerline
e = value at edge of boundary layer
g = gas phase
h = condition at port head end
m = maximum absolute value
s = condition at surface
π = condensed phase, propellant

Superscripts and Operators

$\overline{\quad}$ = average of variable over turbulent fluctuations
$< >$ = time mean of variable
$'$ = turbulent fluctuation value of variable
$''$ = acoustic fluctuation value of variable
$*$ = reference condition

Presented as Paper 88-2942 at the AIAA/ASME/SAE/ASEE 24th Joint Propulsion Conference, Boston, MA, July 11–13, 1988; received Dec. 13, 1988; revision received Aug. 20, 1989.

*Associate Professor, Department of Aeronautical and Astronautical Engineering. Associate Fellow AIAA.
†Graduate Research Assistant. Student Member AIAA.

I. Introduction

PRIOR analytical work on combustion instability in solid rockets has identified some of the mechanisms that can produce velocity-field coupling to the overall instability process (see, for example, the review by Culick[1]). These studies have shown that for a simple longitudinal standing acoustic wave in a duct, a Rayleigh diabatic instability criterion can result, which is dependent upon the oscillatory motion of the gas column. Since the energy release occurs in the near surface

region, analytical work has addressed acoustic boundary-layer effects on propellant combustion response. Implicit in several response function analyses is the assumption that the acoustic boundary layers (Stokes layers) behave quasisteadily and in phase with the longitudinal acoustic velocity outside the boundary layer. For example, the response functions obtained by Lengelle[2] and Gostinsev and Pokhil[3] result from perturbations of the steady-state erosive burning response.

Recent work on combustion-flowfield interactions in solid rocket chambers has analytically and experimentally examined fundamental fluid-dynamic aspects of mean flow, acoustic wave, and turbulence behavior. Hydrodynamically modeling the flow with a semienclosed, porous-walled duct (with large injection through the wall), Brown et al.[4] experimentally confirmed the transitional behavior of the mean flow predicted in Ref. 5. Sankar et al.[6] have obtained schlieren and radiation measurements for a premixed reactive Stokes layer on a porous plate.

Analyses of laminar acoustic boundary-layer phenomena involved in propellant response have been offered by Flandro[7] and Hegde et al.[8] Although several aspects of these analyses are interesting, the following important point is noted. Simple scaling estimates of the laminar acoustic boundary-layer height (the Stokesian thickness) $\delta_a = (\nu/f)^{1/2}$ indicate that δ_a is well above the gas-phase flame height except for very high frequencies ($f \geq 10^4$ Hz). The actual acoustic boundary-layer thickness in the presence of injection, δ_{aa}, can be an order of magnitude larger than δ_a. Consequently, minimal acoustic velocity interaction with combustion would be expected at low to intermediate frequencies as indicated, for example, by the results of Ref. 7. Although this does not preclude "velocity coupled" instability resulting from laminar interactions (whether linear or nonlinear), it does suggest that other mechanisms of interaction should be explored.

Toward this end, the potential for the reactive laminar acoustic boundary layer to undergo transition to turbulence is considered independently of any mean axial flow. It is well established that for piston-driven closed duct flows (viz., in which there is a negligible mean axial flow), longitudinal acoustic waves of a few percent relative pressure amplitude can induce turbulence within the Stokes layer.[9] The recent analysis of Beddini and Roberts[10] yielded appreciable reduction of the critical amplitudes for transition of the nonreactive Stokes layer in the presence of moderate injection velocities. Acoustic turbularization of the propellant combustion zone was also suspected by Medvedev and Revyagin,[11] based upon their T-burner data and the data of Price.[12]

It is known from studies of quasisteady solid propellant/flowfield interactions that even small levels of turbulence within the combustion zone can appreciably enhance propellant combustion rates, predominantly by increasing heat transfer from the flame zone back to the propellant surface. Whether acoustically induced turbularization can occur in actual rocket chambers depends upon several complex effects including the presence of large injection rates, surface roughness, and of course, the specific type of combustion process. The objective of the present analysis is to consider, under several simplifying assumptions, general trends of reactive acoustic boundary-layer turbularization on a propellant surface under nominal homogeneous propellant conditions and to assess the resulting response.

II. Analysis

The motion of a calorically perfect reactive gas described by the Navier-Stokes equations is considered. An arbitrary dependent variable, $g(x_i,t)$ is decomposed according to the notation

$$g(x_i,t) = \bar{g}(x_i,t) + g'(x_i,t)$$

with

$$\bar{g} = <g(x_i,t)> + g''(x_i,t)$$

In these equations, g' is the turbulent fluctuation, $\bar{g}$ is the ensemble average, g'' is the acoustic (deterministic) component, and $<g>$ is the long-time mean. The remainder of this section is divided into three parts; the first will discuss the equations and method used for the numerical solution of the turbulent, reactive, gas-phase, acoustic boundary layer with injection. The second part will discuss the basic assumptions, governing equations, boundary conditions, and mapping technique employed in the unsteady condensed-phase, heat-conduction analysis. The final part will discuss the iterative procedure required to couple the condensed and gas-phase solutions through the gas/solid interface energy balance.

A. Gas-Phase Analysis

The second-order turbulence closure approach developed by Donaldson[13] and Varma et al.[14] was implemented in Ref. 5 as a parabolized model for calculating statistically stationary, compressible, transitional flows in porous walled ducts with large injection rates and in Ref. 15 for the analysis of solid propellant erosive burning. The assumptions and order-of-magnitude analysis of Ref. 10 also yield a one-dimensional time dependent equation system for the present reactive acoustic boundary-layer problem. The assumptions concerning the gas phase are summarized in Table 1. In particular, it is assumed that the Reynolds number based on acoustic velocity and chamber radius is large, that acoustic-turbulence interaction correlations such as $\overline{g'' g'}$ are negligible, and that the axial mean flow Mach number is negligible, as appropriate to a center-vented, T-burner environment and, to a certain sense, the head-end region of a rocket chamber. Additionally, the order-of-magnitude analysis indicates that axial derivatives (with the exception of $\partial\bar{p}/\partial x$) may be neglected if $<M>$ is sufficiently small. It is also required that the acoustic boundary-layer thickness be much less than the characteristic chamber transverse distance ($\delta_a/\delta \ll 1$), a condition that may not be satisfied in test chambers with very small internal radii. The gas-phase equations for the ensemble mean variables are then

$$\frac{\partial\bar{\rho}}{\partial t} + \frac{1}{\rho^{\vartheta}}\frac{\partial}{\partial r}\left[r^{\vartheta}(\bar{\rho}\bar{v} + \overline{\rho' v'})\right] = 0 \qquad (1a)$$

Table 1 Summary of assumptions concerning the gas and condensed phases

Gas-phase assumptions
a) External body forces and the coefficient of bulk viscosity are negligible.
b) Effects of radiation are negligible.
c) Species diffusion due to thermal and pressure gradient effects is negligible, and all binary diffusion coefficients are equal.
d) The Lewis number is unity.
e) Specific heats of the chemical species are equal and independent of temperature.
f) The mean flow Mach number $<M>$ is negligible.
g) The acoustic boundary-layer thickness δa is much smaller than the duct radius or transverse dimension.
h) Combustion of a homogeneous reactant mixture proceeds through a single-step, irreversible, chemical reaction.
i) The gas-phase species-average molecular weight is equal to the molecular weight of the mixture at equilibrium.
Condensed-phase assumptions
a) The condensed phase is homogeneous.
b) The condensed phase is stationary in the reference coordinate system.
c) Material properties are constant.
d) Species diffusion is negligible.
e) Radiation effects at the interface and in the condensed phase are negligible.
f) The surface regression rate is small compared to the gas-phase injection velocity.
g) Subsurface reactions are not present.
h) Surface regression mechanism is governed by the Arrhenius pyrolysis law.

$$\bar{\rho}\frac{\partial \bar{u}}{\partial t} + (\bar{\rho}\bar{v} + \overline{\rho' v'})\frac{\partial \bar{u}}{\partial r} + \frac{1}{r^{\vartheta}}\frac{\partial}{\partial r}(r^{\vartheta}\bar{\rho}\,\overline{u' v'})$$

$$= \frac{1}{r^{\vartheta}}\frac{\partial}{\partial r}\left(r^{\vartheta}\bar{\mu}\frac{\partial \bar{u}}{\partial r}\right) - \frac{\partial \bar{p}}{\partial x} \tag{1b}$$

$$\bar{\rho}\frac{\partial \bar{h}}{\partial t} + (\bar{\rho}\bar{v} + \overline{\rho' v'})\frac{\partial \bar{h}}{\partial r} + \frac{1}{r^{\vartheta}}\frac{\partial}{\partial r}(r^{\vartheta}\bar{\rho}\,\overline{h' v'})$$

$$= \frac{1}{r^{\vartheta}}\frac{\partial}{\partial r}\left(r^{\vartheta}\frac{\bar{k}}{c_p}\frac{\partial \bar{h}}{\partial r}\right) + \frac{\partial \bar{p}}{\partial t}$$

$$+ \bar{\mu}\left[\left(\frac{\partial \bar{u}}{\partial r}\right)^2 + (A + B \cdot Re_t)\frac{q^2}{\Lambda^2}\right] + \Delta h_g \bar{\omega} \tag{1c}$$

where $\Delta h_g \bar{\omega}$ is the energy source term due to a single-step gas reaction, and A and B are constant parameters used in the turbulence model.[5,15] For the present analysis, it has also been assumed that the Lewis number is unity, combustion of a homogeneous propellant occurs in a low Mach number region, and the $\partial \bar{p}/\partial t$ term in the enthalpy equation is negligible (pressure node). Under these assumptions, the species mass fractions needed to evaluate the reaction rate expression are uniquely expressible in terms of enthalpy due to similarity.[15] The expression for ω is then

$$\omega = B_g T^{\beta g} \exp(-T_{Ag}/T)\left[\frac{\rho(H_e - H)}{\Delta h_g}\right]^{\Phi}$$

where

$$\Delta h_g = \sum_{\alpha}(Y_{\alpha *} - Y_{\alpha e})h_{\alpha}^0$$

In the present analysis, $\bar{\omega} = \omega(\bar{T},\bar{\rho})$ since it has been shown that the effects of near-surface turbulent reaction rate correlations are small for homogeneous propellants.[16]

The parabolic differential equation system for the ensemble mean and turbulence variables may be considered in the functional form

$$\bar{\rho}\frac{\partial \bar{g}}{\partial t} + \bar{\rho}\bar{v}\frac{\partial \bar{g}}{\partial r} = \frac{1}{r^{\vartheta}}\frac{\partial}{\partial r}\left(r^{\vartheta}\bar{\mu}_g\frac{\partial \bar{g}}{\partial r}\right) + G(g) \tag{2}$$

where $g = \{\bar{u}, \bar{h}, \overline{u'u'}, \overline{v'v'}, \overline{w'w'}, \overline{u'v'}, \overline{h'u'}, \overline{h'v'}, \overline{h'h'}\}^T$; u, v, and w are the axial, radial, and circumferential velocity components, ϑ the index for planar or axisymmetric geometry, ρ the density, and $h = c_p T$ the specific static enthalpy. The molecular transport coefficient μ represents the dynamic viscosity (μ) or the thermal conductivity parameter, $\sigma = k/c_p$, as appropriate for each equation. However, not all of the molecular diffusion terms for each equation in the system may be cast in the form shown in Eq. (2). Those that do not conform are implicitly contained within the complex functions G, which also represent the sources, cross-coupling, and dissipation terms for the equations.

The pressure along the chamber, $\bar{p} = <p> + p''(x,t)$, is specified by the one-dimensional standing wave solution

$$p'' = \Pi_{ma} <p> \cos(n\pi x/L)\cos(2\pi f t)$$

where Π_{ma} is the maximum relative acoustic pressure amplitude, and $x/L = 1/2$ (pressure node). The maximum acoustic axial velocity (outside the boundary layer) is $u_{ma} = \Pi_{ma}\, a_0/\gamma$.

The turbulence length scale Λ in this model is algebraic and described[5] by a linear variation from its surface value, Λ_s ($\Lambda_s = 0$ for smooth walls) to a plateau level proportionate to the thickness of the shear flow. For the present analysis, this thickness was defined as δ_{aa}, equal to the height above the surface where the first-zero crossing of u'' occurs.[9] The final values of δ_{aa} used in the length scale expression were smoothed by temporal averaging.

Boundary conditions at the chamber centerline (or centerplane) are the symmetry conditions, which for the posed system are

$$\frac{\partial}{\partial r}(\bar{u}, \bar{h}, \overline{u'u'}, \overline{v'v'}, \overline{w'w'}, \overline{u'v'}, \overline{h'u'}, \overline{h'v'}, \overline{h'h'}) = 0$$

$$\overline{u'v'} = \overline{h'v'} = 0$$

Because of the final form of the governing equations, the requirement that $\bar{v} = 0$ on the centerline (centerplane) is necessarily relaxed since it would otherwise create a mean pressure gradient and axial flow. At the chamber surface, the static enthalpy corresponding to the surface temperature and the mean injection velocity, $\bar{v}_s$, are determined from an iterative procedure using the energy balance at the gas/solid interface (see the following section). The no-slip condition implies that all tangential velocity components and their correlations are zero.

B. Condensed-Phase Analysis

The unsteady condensed-phase heat conduction is determined through a coupled numerical solution of the gaseous and condensed phases employing an iterative procedure based on the gas/solid interface energy balance. The condensed-phase coordinate η runs from zero at the gas/solid interface to $-\infty$ in depth. The gas-phase coordinate y runs from zero at the gas/solid interface to $+\infty$. The assumptions concerning the condensed phase are summarized for convenience in Table 1. The condensed-phase heat conduction equation, in the absence of subsurface reactions, is

$$\frac{\partial T}{\partial t} + \dot{r}\frac{\partial T}{\partial \eta} = \alpha_{\pi}\frac{\partial^2 T}{\partial \eta^2} \tag{3}$$

An energy balance at the gas/solid interface yields the boundary condition at $\eta = 0$:

$$k_g \left.\frac{\partial T}{\partial y}\right|_s - k_{\pi}\left.\frac{\partial T}{\partial \eta}\right|_s = \rho_{\pi}\dot{r}\left[T_s(c_p - c_{\pi}) + L_s^0\right] \tag{4}$$

where the enthalpy of decomposition is

$$L_s^0 \equiv \sum_{\text{(reactants)}}\left(h_{\alpha}^0\right)_g - h_{\pi}^0$$

In Eq. (4), the assumption of large chamber radius is made for convenience. Equations (3) and (4) are both nonlinear because the surface regression rate $\dot{r}$ is a strong function of the surface temperature T_s. The regression rate (determined by the condensed-phase sublimation or evaporation) is assumed to be governed by an Arrhenius pyrolysis law of the form

$$\dot{m} = \bar{\rho}_s \bar{v}_s = \rho_{\pi}\dot{r} = A_s e^{-T_{As}/T_s} \tag{5}$$

Finally, the in-depth boundary condition is simply

$$\eta \to -\infty, \qquad T \to T_{\pi} \tag{6}$$

where T_{π} is the constant in-depth propellant temperature.

Equations (2–6) completely specify the unsteady conduction of heat into the condensed phase. The solution is obtained by performing a linear coordinate transformation on Eqs. (3) and (4) to map the condensed phase onto the computational gas-phase grid. Equation (3) and the gas-phase equations (1) are then solved numerically, using the Crank-Nicolson, finite-difference method, and Eq. (4) is used to iteratively solve for the interface surface temperature. The linear transformation from η space to y space is

$$y = -(1/\zeta_{\pi})\eta \tag{7}$$

where $\zeta_\pi = k_\pi c_p/[k(T_s)c_\pi)]$ is a scaling parameter used to approximately match the depth of the combustion wave in the condensed-phase to the flame height in the gas phase. This transformation enables the condensed-phase solution to take full advantage of the dynamically adaptive gas-phase grid and ensures consistent numerical treatment. Applying the transformation to Eqs. (3), (4), and (6) produces the following system of equations:

$$\frac{\partial T}{\partial t} - \frac{\dot{r}}{\zeta_\pi}\frac{\partial T}{\partial y} = \frac{\alpha_\pi}{\zeta_\pi^2}\frac{\partial^2 T}{\partial y^2} \tag{8a}$$

$$k_g\left(\frac{\partial T}{\partial y}\bigg|_s\right)_g + \frac{k_\pi}{\zeta_\pi}\left(\frac{\partial T}{\partial y}\bigg|_s\right)_\pi = \rho_\pi \dot{r}\left[T_s(c_p - c_\pi) + L_s^0\right] \tag{8b}$$

$$y \to +\infty, \qquad T \to T_\pi \tag{8c}$$

C. Iterative Coupling Procedure

The gas/solid interface energy balance, Eq. (8b), and the pyrolysis relation, Eq. (5), provide the coupling between the condensed- and gas-phase solutions. The coupled solution is obtained by an iteration process (here referred to as a substep) at the new time step as follows:

1) Condensed- and gas-phase solutions are obtained using the values of the gas/solid interface temperature and mean injection velocity specified at the previous temporal step or substep.

2) An updated interface mass flux is specified using Eq. (8b) and is obtained from

$$(\dot{m}_s)|_{n+1} = (\rho_\pi \dot{r})|_{n+1}$$

$$= \left\{\left[k_g\left(\frac{\partial T}{\partial y}\bigg|_s\right)_g + \frac{k_\pi}{\zeta_\pi}\left(\frac{\partial T}{\partial y}\bigg|_s\right)_\pi\right]\left[T_s(c_p - c_\pi) + L_s^0\right]^{-1}\right\}\bigg|_n$$

where n and $n+1$ are the nth and $n+1$st substeps, respectively.

3) Equation (5) is inverted to obtain the corresponding surface temperature

$$(T_s)|_{n+1} = -T_{As}/\ell n\left\{\frac{(\dot{m}_s)|_{n+1}}{A_s}\right\}$$

and the updated gas-phase injection velocity is determined from

$$(\bar{v}_s)|_{n+1} = (\dot{m}_s)|_{n+1}/\rho_g)_s$$

4) The condensed and gas phases are solved once again using the updated values, and the process is repeated until convergence is achieved (typically two or three iterations).

III. Discussion of Results

The thermochemical properties and reference operating conditions of the baseline solid propellant, presented in Table 2, were chosen to represent the nominal properties of homogeneous propellants and were also used in the erosive burning study of Ref. 14. Calculations presented were performed using the baseline propellant, which has an exothermic surface reaction and an identical propellant with an endothermic surface reaction, $L_s^0 = 837$ J/kg. To reproduce the reference operating conditions, the pre-exponential constant in the gas-phase reaction rate was calculated to be 8.2×10^9 $\text{kg}^{1-\Phi}\text{m}^{\Phi-1}\text{s}^{-1}\text{K}^{Bg}$ for the endothermic propellant. Steady-state calculations performed over a broad range of pressures yielded a normal rate of regression $\dot{r} = \dot{r}^*(p/p^*)^n$ with $\dot{r}^*$ and n as indicated in the Table 2. Transition calculations were performed using 50 time steps per cycle and two iterations per step, and propellant response calculations were performed using 100 steps per cycle and three iterations per step. Unless stated otherwise, all propellant responses were obtained at an acoustic frequency of 1000 Hz and 5% acoustic pressure ratio $\Pi_{ma} = 0.05$. The disturbance level of the gas transpiring from the propellant surface σ_v was assumed to be zero in all calculations (see Ref. 10).

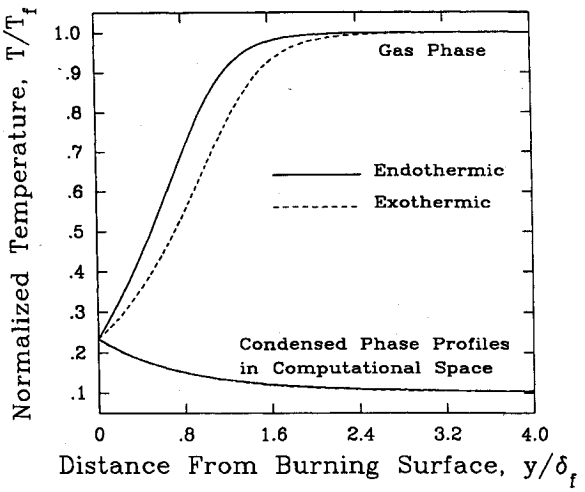

Fig. 1 Steady-state temperature profiles.

Shown in Fig. 1 are the normalized steady-state temperature profiles obtained in the gas and condensed phases for the endothermic and exothermic propellant formulations at reference conditions normalized by the approximate theoretical gas-phase flame height δ_f (note that the approximate δ_f scaling used here is independent of L_s^0). The results indicate that the exothermic formulation provides an anticipated increased gas-phase flame height increasing the possibility of acoustically induced turbulence interacting with the flame zone. The coincident condensed-phase profiles are shown plotted in the gas-phase computational coordinates and are therefore scaled by $\zeta_\pi = 4.0$ in all calculations.

Thus, if the scaling were not employed, the condensed-phase combustion wave would be approximately four times the length of the flame zone, and the condensed-phase solution would not efficiently use the dense grid (generally 35 points) provided by the dynamically adaptive grid within the combustion zone.

Figure 2 presents the normalized temperature and turbulent velocity profiles vs distance from the burning surface. The abscissa is normalized by $\delta_a = 100$ μm. The profiles are given for various times within the acoustic cycle for the baseline propellant with an equivalent sand roughness of $k_s = 150$ μm. The abscissa is presented as a logarithmic scale to reveal the

Table 2 Thermochemical parameters for baseline propellant

T_f	2976 K
c_p	1.92×10^3 J/kg-K
W_{av}	25.8 kg/kg-mole
T_{Ag}	2.0×10^4 K
B_g	6.5×10^9 $\text{kg}^{1-\Phi}\text{m}^{\Phi-1}\text{s}^{-1}\text{K}^{-\beta g}$
Φ	1.10
β_g	0
μ	4.42×10^{-7} $(T)^{0.65}$ kg/m/s/$\text{K}^{0.65}$
Pr	1
T_π	300 K
L_s^0	-4.184×10^5 J/kg (-100 cal/g)
ρ_π	1700 kg/m^3
c_π	1.46×10^3
A_π	2.5×10^7 kg/m^2 – s
$T_{A\pi}$	1×10^4 K
$\dot{r}$	9.2×10^{-3} m/s
T_s^*	700 K
p^*	68 atm
n	0.55

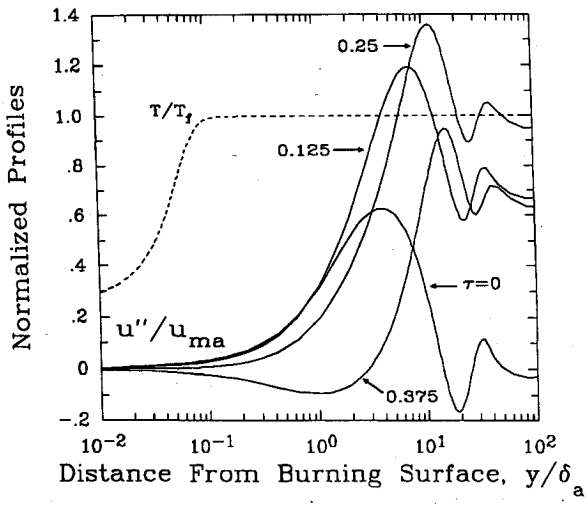

Fig. 2 Comparison of temperature and turbulent velocity profiles at various times within a cycle.

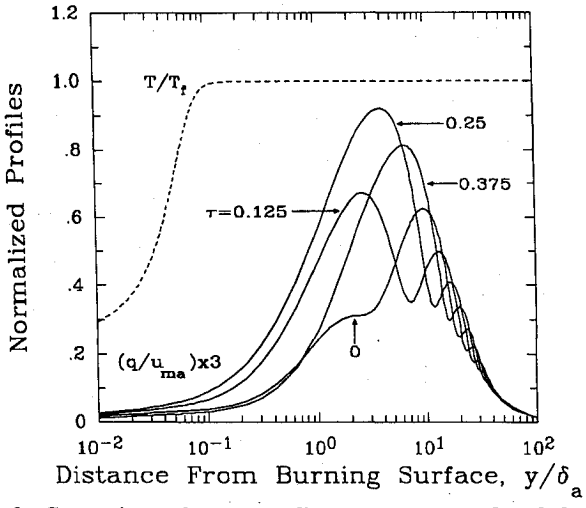

Fig. 3 Comparison of corresponding temperature and turbulence intensity profiles at various times within a cycle.

details in the near-surface flame region. The results obtained show the phase shift and Richardson annular effect due to viscosity and injection that were obtained in previous studies[10] of isothermal Stokes layers. The acoustic velocity is negligible in the region of the flame zone at this intermediate frequency. However, Fig. 3 shows the corresponding normalized temperature profiles and turbulence intensity profiles. The peaks in turbulence intensity within the cycle correspond approximately to the large velocity gradients produced by the Richardson annular effect. The results indicate that the turbulence intensity obtains magnitudes of 1–2% within the combustion region at certain points within the acoustic cycle and results in propellant combustion responding to enhanced heating rates due to turbulent diffusion.

In Ref. 9, it was found that for a smooth surface ($k_s = 0$) without surface injection disturbances ($\sigma_v = 0$), an acoustic transition locus could be expressed in terms of axial acoustic velocity Reynolds number as a function of an injection velocity acoustic Reynolds number. Figure 4 shows the previously reported results. The critical amplitude locus is quite sensitive to the method used to introduce "seed" turbulence into the boundary layer and to other conditions such as the relative height within the boundary layer at which amplification is determined.[10] Figure 4 shows additional calculations for an isothermal boundary layer, which utilize an alternative means of introducing the initial disturbance. (The difference between the two methods is that the earlier results introduced a 1% peak disturbance level within the Stokes layer thickness δ_a, whereas the present results introduce the same 1% disturbance level over the much larger actual injected boundary-layer thickness, δ_{aa}.)

Using this new and perhaps more realistic method, transition calculations were also performed for the baseline propellant at frequencies of 100 and 1000 Hz over pressures ranging from 10 to 100 atmospheres. The transition points obtained for propellant combustion are in good agreement with the isothermal calculations. Thus, the appropriate scaling involves flame or edge quantities only and indicates that the acoustic flowfield (for a smooth surface) can be approximated as an isothermal flow at the steady-state flame temperature in determining transition.

Figure 5 shows the calculations presented in Fig. 4 for the endothermic propellant along with calculations for the exothermic propellant at an acoustic frequency of 100 Hz plotted as a function of the critical acoustic pressure ratio Π_{cr} vs the mean pressure normalized by p^*. The critical pressure ratio is found to be insensitive to the heat released from the surface reaction, although the actual response of the propellant is dependent on L_s^0. This results because, for a smooth wall, transition is initiated above the thin combustion zone. The critical pressure ratio is found to decrease with increasing mean pressure in all cases indicating that a propellant that may be stable with respect to a specific acoustic mode at a known mean pressure may encounter acoustic transition at that mode when operating at an elevated mean pressure. This phenome-

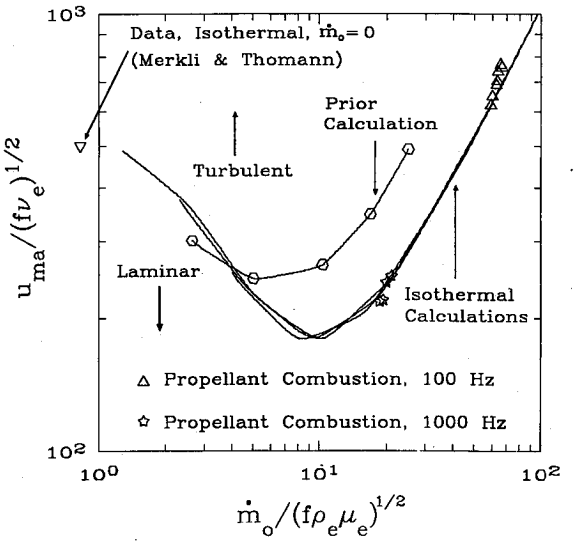

Fig. 4 Critical acoustic Reynolds number required for transition.

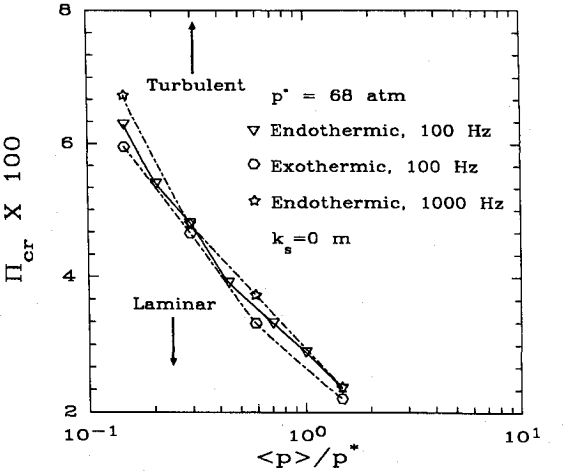

Fig. 5 Variation of critical pressure ratio required for transition as a function of mean chamber pressure.

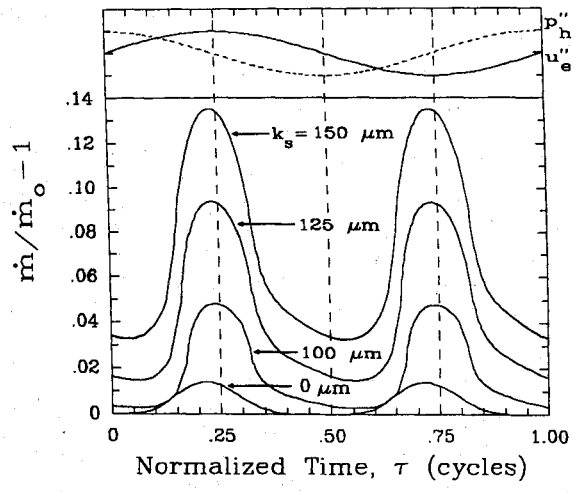

Fig. 6 Variation of propellant response as a function of time for various surface roughness heights.

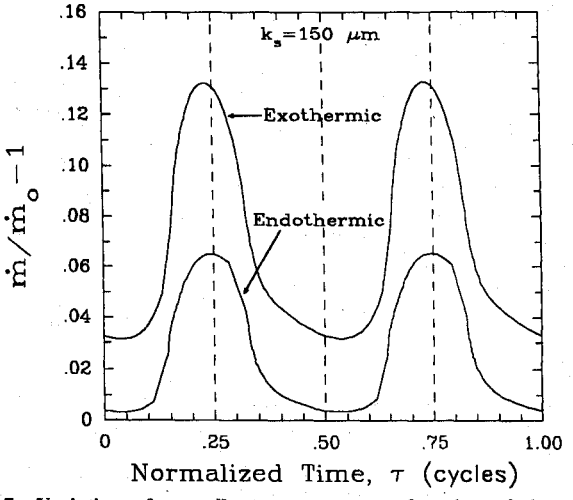

Fig. 7 Variation of propellant response as a function of time for endothermic and exothermic surface decomposition energies.

non may explain stability problems encountered in the development of solid rocket motors with unconventionally high chamber pressures.

Figure 6 shows the response of the baseline endothermic propellant to the presence of the turbulent acoustic boundary layer for various surface roughnesses. The normalized propellant mass flux (burn rate) is plotted vs normalized time τ. A diagram of the variation of the acoustic edge velocity and pressure is included at the top of the figure. The pressure variation is correct for an axial location in the head-end region of a chamber. In the aft-end region, the pressure would be shifted 180 deg in phase with respect to the pressure curve shown. The case of a smooth wall $k_s = 0$ m required a 15% pressure ratio to obtain the response shown. The cases in which a finite value of surface roughness was prescribed were calculated using a 5% pressure ratio. The smooth wall produced only a slight response in the propellant burn rate that is rectified with respect to the velocity field and that is negligible over a large portion of each half cycle. The calculations in which finite levels of surface roughness are included reveal several interesting features. All cases exhibit the rectified response along with a time-mean augmentation (D-C shift) of the propellant burn rate, about 8% for $k_s = 150$ μm, 5% for 125 μm, and 2% for the 100-μm surface roughness. The relative phase of the response, with respect to the acoustic velocity and pressure field, varies with surface roughness and may provide a mechanism by which the acoustical energy can be reinforced or damped according to the Rayleigh criterion.

Figure 7 compares the effect of surface decomposition energy on the propellant response. The calculations were performed for the endothermic and exothermic propellant formulations with $k_s = 150$ μm and $\Pi = 0.05$ in both cases. The exothermic propellant has a mean shift in burning rate that is approximately three times as large as that occurring in the endothermic case.

The propellant's response to the acoustic boundary layer is further investigated using a conventional fast Fourier transform (FFT) analysis over several cycles. The cases examined are identical to the calculations with finite roughness presented in Fig. 6 and discussed above. Figures 8 and 9 present the results of the analysis in terms of the relative amplitude and frequency content of the response and the relative phase of the responses at each frequency, respectively. The large dashed curve is the driving frequency of the external acoustic velocity, the small dashed curve is the response of the propellant with a smooth wall (the response has been shifted positive 300 Hz to facilitate the comparison), and the solid curve is the response with $k_s = 150$ μm. The frequency content and relative amplitudes of the response with $k_s = 150$ μm is representative of the cases with finite surface roughness. The results presented in Fig. 8 have, in each case, been normalized by the largest amplitude obtained for that calculation after removal of the zero-frequency component. It can be seen that in both calculations the primary response occurs at the second harmonic with significant harmonic content occurring at the lower, even harmonics. Only even harmonics are obtained in

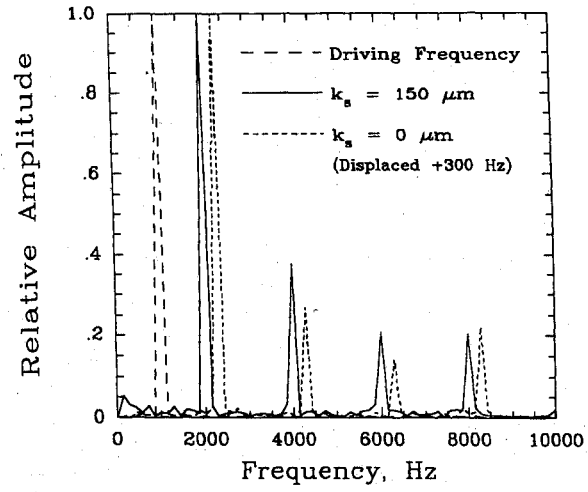

Fig. 8 Harmonic content of the propellant responses shown in Fig. 6 for a smooth and rough wall ($k_s = 0$ and $k_s = 150$ μm, respectively).

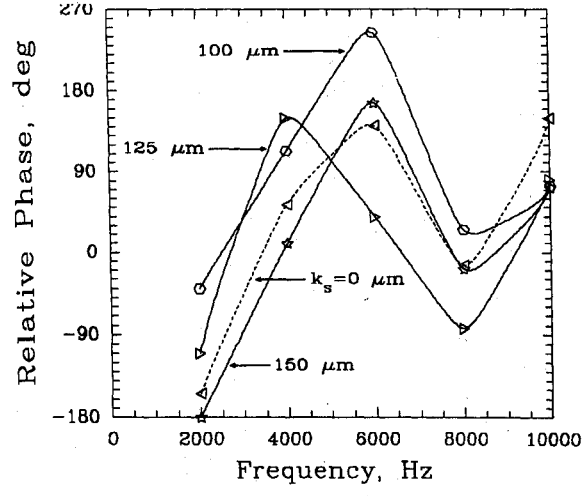

Fig. 9 Relative phase angle of the responses shown in Fig. 6.

the present study since axial mean flow is neglected, and calculations are performed at a pressure node. The relative phase of the propellant response, presented in Fig. 9, is seen to vary substantially from harmonic to harmonic. It can further be seen that at the second harmonic, 2000 Hz, the phase lag of the response increases with increasing surface roughness (excluding the smooth wall case due to the large pressure ratio required to obtain the response).

IV. Conclusions

The analysis presented in this work has attempted to identify and quantify the role of acoustically induced turbulence in the combustion response of solid propellants. Despite several simplifying assumptions, a complex nonlinear and spatially dependent interaction occurs in the reaction zone, which produces an analogously complex response function. Some features of the response have long been hypothesized (see, for example, Ref. 1) and are presently analytically confirmed, viz. "full wave" rectification relative to the harmonic acoustic velocity outside the boundary layer, the occurrence of a threshold acoustic amplitude for significant response, and the appearance of a time-mean augmentation (D-C shift) of the propellant regression rate. Additionally, the magnitude of the response is quite sensitive to propellant "formulation variables"; surface roughness and gas-phase heat of reaction (flame-zone thickness) are those assessed in this study.

The results also indicate differences with some prevailing conceptual aspects of velocity coupled response. These include the following:

1) The response to acoustic velocity oscillations can be independent of steady-state erosive burning, as demonstrated by the neglect of an appreciable axial mean flow in this analysis. Consequently, contemporary treatments of velocity response functions, which simply perturb an erosive burning response, would omit an important additional contribution and physical mechanism.

2) For nominal combustion parameters, the susceptibility to acoustic transition and propellant response increases with increasing mean pressure.

3) The appreciable phase shift of the regression rate response relative to the harmonic external axial velocity can yield a significant "apparent" pressure response, if an attempt was made to analyze this with conventional linear theory.

4) The behavior of the velocity response, even at moderate acoustic pressure amplitudes of a few percent, is highly nonlinear and possesses significant harmonic content.

The present results have been obtained using several simplifying assumptions, some of which pose significant research issues in their own right (for example, the potential for direct acoustic-turbulence interaction, the potential for extreme combustion-turbulence interaction from composite-propellant diffusion flamelets, or the additional propellant-dependent characteristic of exothermic reactions within the condensed phase). One of the more intriguing questions posed by the present results is the potential influence of an axial mean flow interacting with the acoustic boundary layer and turbulence fields. In this case a substantial biasing of the propellant response over a cycle is anticipated (a necessary condition for instability). Considering the sensitivity and nonlinearity of the acoustic transition process obtained in the present study, this area of research could provide critical insight into the coupling mechanisms producing instability in actual propulsion chambers.

Acknowledgments

This research has been supported by the Air Force Astronautics Laboratory under Contract F04611-86-K-0081 and by the Air Force Office of Scientific Research under Grant 86-0319. The authors would like to acknowledge the assistance of graduate research assistants Jeffrey P. Ridder and Joseph S. Wood in the preparation of graphics and manuscript, and the National Center for Supercomputing Applications for the use of their computing facilities.

References

[1]Culick, F. E. C., "A Review of Calculations for Unsteady Burning of a Solid Propellant," *AIAA Journal,* Vol. 6, No. 12, 1968, pp. 2241–2255; also "Stability of Longitudinal Oscillations with Pressure and Velocity Coupling in a Solid Propellant Rocket," *Combustion Science and Technology,* Vol. 2, No. 4, pp. 179–201.

[2]Lengellé, G., "A Model Describing the Velocity Response of Composition Propellants," *AIAA Journal,* Vol. 13, No. 11, 1975, pp. 315–322.

[3]Gostinsev, Y. A., and Pokhil, P. F., "Relation of Two Combustion Anomalies of Powder Tubes," *Doklady Akademii Nauk SSSR, (Soviet Physics—Doklady)*, Vol. 188, No. 1, 1969, pp. 135, 136.

[4]Brown, R. S., Willoughby, P. G., and Dunlap, R., "Coupling Between Velocity Oscillations and Solid Propellant Combustion," *Journal of Propulsion and Power,* Vol. 2, No. 5, 1986, pp. 428–437.

[5]Beddini, R. A., "Injection-Induced Flows in Porous Walled Ducts" *AIAA Journal,* Vol. 24, No. 11, 1986, pp. 1766–1773.

[6]Sankar, S. V., Jagoda, J. I., Daniel, B. R., and Zinn, B. T., "Flame-Acoustic Wave Interaction During Axial Solid Rocket Instabilities," AIAA Paper 86-0532, Jan. 1986.

[7]Flandro, G. A., "Non-Linear Transient Combustion of a Solid Rocket Propellant," AIAA Paper 83-1269, June 1983.

[8] Hegde, U. G., Chen, F. L., and Zinn, B. T., "Investigations of the Acoustic Boundary Layer in Porous Walled Ducts with Flow," AIAA Paper 85-0078, Jan. 1985.

[9]Merkli, P., and Thomann, H., "Transition to Turbulence in Oscillating Pipe Flow," *Journal of Fluid Mechanics,* Vol. 68, Pt. 3, April 1975, pp. 567–575.

[10]Beddini, R. A., and Roberts, T. A., "Turbularization of an Acoustic Boundary-Layer on a Transpiring Surface, *AIAA Journal,* Vol. 26, No. 8, 1988, pp. 917–923.

[11]Medvedev, Y. I., and Revyagin, L. N., "Unsteady-State Erosion of a Powder," *Fizika Goreniya i Vzryva,* Vol. 10, No. 3, 1974, pp. 341–345.

[12]Crump, J. E., and Price, E. W., Effects of Acoustic Environment on the Burning Rate of Solid Propellants," *AIAA Journal,* Vol. 2, No. 7, 1964, pp. 1274–1278.

[13]Donaldson, C., "Calculations of Turbulent Shear Flows for Atmospheric and Vortex Motions," *AIAA Journal,* Vol. 10, No. 1, 1972, pp. 4–12.

[14]Varma, A. K., Beddini, R. A., Sullivan, R. D., and Donaldson, C., "Application of an Invariant Second-Order-Closure Model to the Calculation of Compressible Boundary Layers," AIAA Paper 74-0592, June 1974.

[15]Beddini, R. A., "Aerothermochemical Analysis of Erosive Burning in a Laboratory Solid-Rocket Motor," *AIAA Journal,* Vol. 18, No. 11, 1980, pp. 1346–1353.

[16]Beddini, R. A., "Analysis of Injection-Induced Flows in Porous-Walled Ducts with Application to the Aerothermochemistry of Solid-Propellant Motors," Ph.D. Thesis, Rutgers Univ., New Brunswick, NJ, Oct. 1981.